14th International Symposium on Turbulence and Shear Flow Phenomena (TSFP14)
Heidelberg, Germany, July 28–31, 2026

LYAPUNOV SPECTRUM OF THE RAYLEIGH-TAYLOR INSTABILITY

Rachel E. Mead
Department of Aerospace Engineering
University of Michigan
Ann Arbor, Michigan 48109, USA
merachel@umich.edu

Daniel M. Israel
Continuum Models and Numerical Algorithms
Los Alamos National Laboratory
Ann Arbor, Michigan 48105, USA
dmi1@lanl.gov

Venkat Raman
Department of Aerospace Engineering
University of Michigan
Ann Arbor, Michigan 48109, USA
ramanvr@umich.edu

ABSTRACT

Numerous studies have used large eddy simulations and direct numerical simulations to investigate how the initial conditions of the Rayleigh-Taylor instability (RTI) affect parameters such as the growth rate. The RTI is chaotic and small perturbations to the system introduced in experiments and simulations can grow to significantly affect the system. This study uses a pseudo-spectral DNS code to take a dynamical systems approach to gain new insight into the extent of the effect of the initial conditions by determining how perturbations grow. The Lyapunov exponents and vectors of the RTI will be used to determine how the perturbation growth changes between different initial conditions and the RTI regimes.

BACKGROUND

The Rayleigh-Taylor instability (RTI) occurs when a light fluid accelerates into a heavy fluid due to a constant acceleration at an unstable interface with an infinitesimal perturbation. The RTI has distinct growth regimes: the diffusive regime, the linear regime, the non-linear regime, and the late-time regime. In the diffusive regime, diffusion dominates and no instability is observed as it must overcome the diffusive layer. In the linear regime, bubbles and spikes begin to form, the modes independently evolve, and the mixing layer height exponentially grows. The linear regime in this study also includes the weakly non-linear regime, where small wavelengths begin to saturate, because the mixing layer height still grows exponentially. In the non-linear regime, nonlinearities also develop as the modes begin to interact with each other due to the shear from the rising and falling fluids, and Kelvin-Helmholtz instabilities begin to form, triggering a transition to turbulence (Cook *et al.*, 2004). At late times, the RTI enters the late-time regime, and the growth rate plateaus. This regime is hypothesized to be self-similar (Ristorcelli & Clark, 2004).

The RTI appears in many contexts including shock-droplet interaction, astrophysics, combustion, and inertial confinement fusion (ICF). Controlling the RTI is important for ICF because the generated mixing reduces the energy yield. The RTI is highly sensitive to the initial conditions and although many studies have shown that changes to the infinitesimal perturbation can affect the growth rate and other fluid flow quantities, fewer studies have focused on the extent to which the effects of the initial conditions last. Of the studies exploring this aspect of the RTI, Thévenin & Gréa (2025) used neural networks to determine that the late-time growth rate loses most if not all dependence on the initial conditions while the virtual time origin of the mixing layer is highly sensitive to the initial conditions. Kord & Capecelatro (2019) instead used a discrete adjoint-based method to determine the sensitivity of the RTI to objective functions to control the growth rate and mixing through the initial conditions. They found that including lower wavenumber modes enhances late time growth rates, including wavenumbers near the most unstable wavelength affects the linear and early non-linear regimes the most, and optimizing for early times does not control mixing at late times.

Understanding the sensitivity of the RTI to initial conditions and perturbations is important, as both experiments and simulations can introduce small perturbations. Lyapunov exponents (LEs) and Lyapunov vectors (LVs) can quantify how perturbations change the solution. Together, the LEs and LVs form the Lyapunov spectrum. The LEs, or λs, describe the exponential rate of stretching (positive) or contracting (negative) in specific directions dictated by each exponent's respective LV (Kalnay, 2002). These values are time-averaged over the entire simulation. Each LE can be interpreted as the inverse time scale over which a perturbation is amplified in a specific direction. The largest LE determines the time over which a prediction with a specified uncertainty is valid for the overall system.

Although the LEs are often used for ergodic systems, such as the low Reynolds number turbulent channel flow calculated by Keefe *et al.* (1992), they can be used for non-ergodic and non-stationary systems, but their meanings change. LEs require ergodicity to be independent of the initial conditions. The LEs of non-ergodic, stationary systems change depending on the initial conditions. A distribution, or probability distribution function (PDF), is obtained when several initial conditions are used (Nath *et al.*, 2024). On the other hand, a system must be statistically stationary to take long-time averages. Often for non-stationary systems, the simulation time is divided into epochs, short time periods over which the system can be approximated as stationary, and therefore over which the LEs can be calculated (Serquina *et al.*, 2008). Therefore, even though the RTI is non-stationary, and therefore non-ergodic, LEs can still be calculated.

In addition to the LEs, the LVs also provide a lot of information. The LVs are instantaneous quantities and can be defined in numerous ways. The Gram-Schmidt vectors, named after the method used, are used in this study. The LVs describe the system's response to perturbations and the evolution of the tangent space to the attractor (Hassanaly & Raman, 2019). The first LV is the most chaotic, while the last computed LV is the least chaotic and tends to be more spatially distributed. In various chaotic systems, it has been shown that most of the perturbation growth occurs in only a small part of the physical space, a property called localization (Hassanaly & Raman, 2019). To investigate the response of the RTI to perturbations, the distribution of elements or combinations of each LV's elements can be compared against the distribution of other flow field variables as done in Hassanaly & Raman (2019) for homogeneous isotropic turbulence. If a flow field variable's distribution highly correlates with the LVs, then that flow variable likely affects the perturbation growth in the RTI.

Using the LEs and LVs, this study aims to better understand how perturbation growth changes between different initial conditions and the different RTI regimes, deepening the current understanding of the physics behind the growth of the RTI and the extent of the effect of the initial conditions. To achieve these goals, this study will utilize pseudo-spectral direct numerical simulations of the Navier-Stokes equations under the Boussinesq approximation and Bennettin's algorithm, which is discussed below, to perform a Lyapunov analysis of the RTI for different initial conditions.

CONFIGURATION

Each simulation will have a domain size of 32π x 32π x 128π with periodic boundary conditions imposed on each boundary. This study will use the characteristic scales for non-dimensionalization,

$$\ell_c = \left(\frac{\nu^2}{gA}\right)^{\frac{1}{3}}, \qquad t_c = \left(\frac{\nu}{g^2A^2}\right)^{\frac{1}{3}}, \qquad u_c = (\nu g A)^{\frac{1}{3}} \quad (1)$$

and the initial perturbation energy spectrum formulation

$$E_n(\kappa) = <\xi\xi>_o \frac{\left(\frac{\kappa}{\kappa_c}\right)^n \exp\left(-\frac{1}{2}a\left(\frac{\kappa}{\kappa_c}\right)^2\right)}{\int_0^\infty \left(\frac{\kappa}{\kappa_c}\right)^n \exp\left(-\frac{1}{2}a\left(\frac{\kappa}{\kappa_c}\right)^2\right) d\kappa} \quad (2)$$

used in Ristorcelli & Clark (2004), where ν is the kinematic viscosity, g is the acceleration, A is the Atwood number, κ_c is the peak of the spectrum, a and n are parameters that change the shape of the spectrum, and $\langle\xi\xi\rangle_o$ is the initial interfacial variance of the grid spacing. The Schmidt number is set to 1 and the non-dimensionalization above sets the computational Reynolds number to 1 and the initial most unstable wavelength to 4π. In order to create different initial conditions, κ_c is varied while keeping $\langle\xi\xi\rangle_o = 0.25$ and $a = n = 2$. The κ_c values of 2, 8, and 16 are used and, respectively, set the initial perturbation energy spectrum peak to a wavelength longer than, equal to, and shorter than the initial most unstable wavelength. Each mode is given a random phase between 0 and 2π.

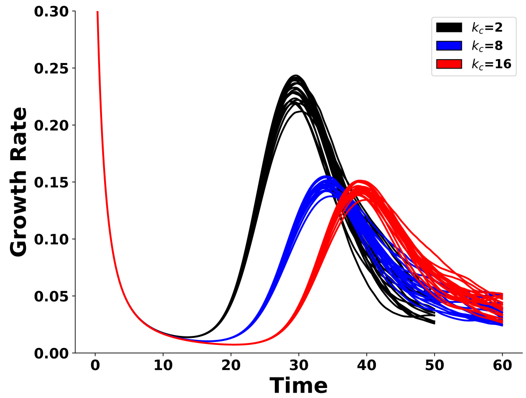

Figure 1: Growth rate of the RTI for each value of κ_c. Each value of κ_c was run twenty times, each with a different random phase of the same perturbation energy spectrum.

COMPUTATION OF LYAPUNOV SPECTRUM

The LEs and LVs are calculated using Benettin's algorithm (Benettin *et al.*, 1980*a*,*b*). For a system of dimension D, there are D LEs and D LVs of dimension Dx1. To calculate the system's first m LEs in decreasing order, m+1 simulations are propagated: one base solution and m trajectories with slightly perturbed initial conditions. The incompressibility condition is enforced through a Poisson equation at the end of each time step. The perturbations have the same small magnitude of 1e-3 for each simulation, form an orthogonal basis, and are the instantaneous LVs when reorthonormalized. The reorthonormalization occurs every 5 time steps due to the exponential growth of the perturbations. The system cannot be reorthonormalized too frequently, as the perturbations must be able to grow, nor too intermittently, as the perturbations will no longer be small. Unlike many non-stationary systems, the LEs are not time-averaged in an epoch. It was determined that the LEs were continuously evolving and that important information would be removed by time-averaging. Instead, several random seeds were used for the phase of the initial perturbation and averaged, while also showing the range of values. These LEs will be called instantaneous LEs.

RESULTS

Twenty simulations for each value of κ_c are run with a coarse 32x32x128 grid until the non-dimensional time $t = 50$ for $k_c = 2$ and $t = 60$ for the other two initial conditions. A time step of $\Delta t = 0.01$ was used for all simulations. The growth rate

$$\alpha = \dot{h}^2/4Agh \quad (3)$$

of each simulation is shown in Figure 1. The concentrations on the x mid-plane of the RTI for one of the random seeds with $\kappa_c = 2$ in the linear, non-linear, and late-time regimes are shown in Figure 2. The main features in the concentration surfaces are similar between random seeds and between κ_c values at similar positions in the growth rate plot.

Effect of Initial Perturbation Spectrum

Figure 3 shows the instantaneous LEs at different times. Figure 3a compares the instantaneous LE spectra between the

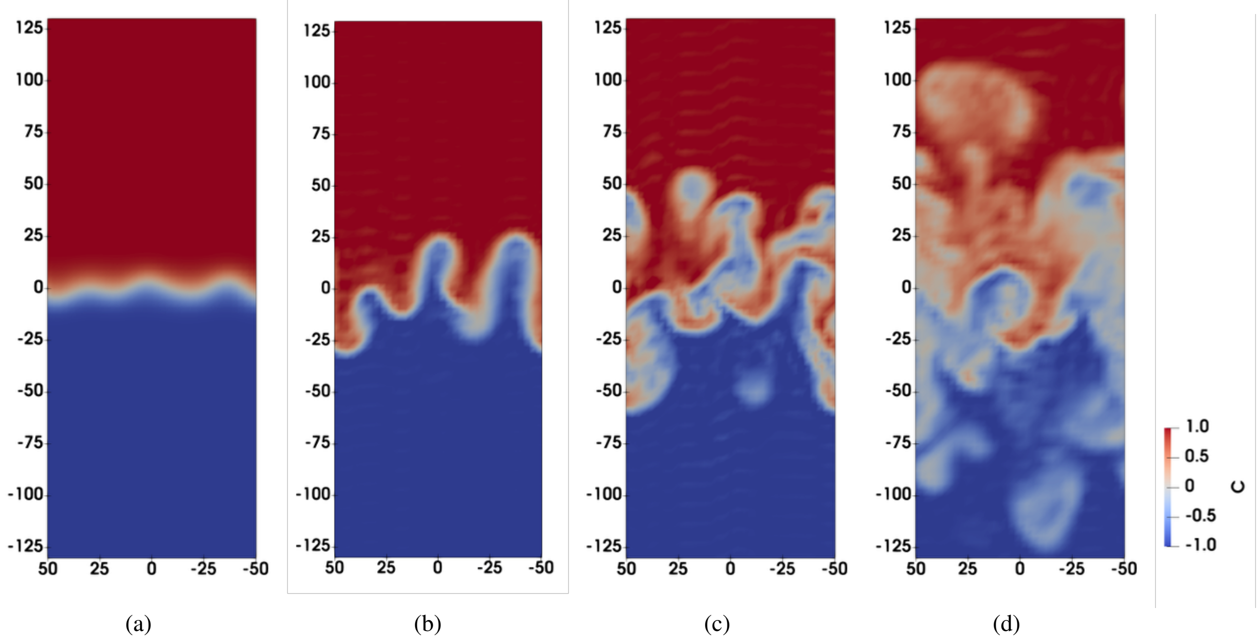

Figure 2: The concentration is shown at the mid-plane of one random seed with the initial condition $\kappa_c = 2$ at times (a) $t = 17$ (linear regime), (b) $t = 29$ (peak growth rate), (c) $t = 37$ (non-linear regime), and (d) $t = 50$ (late-time regime).

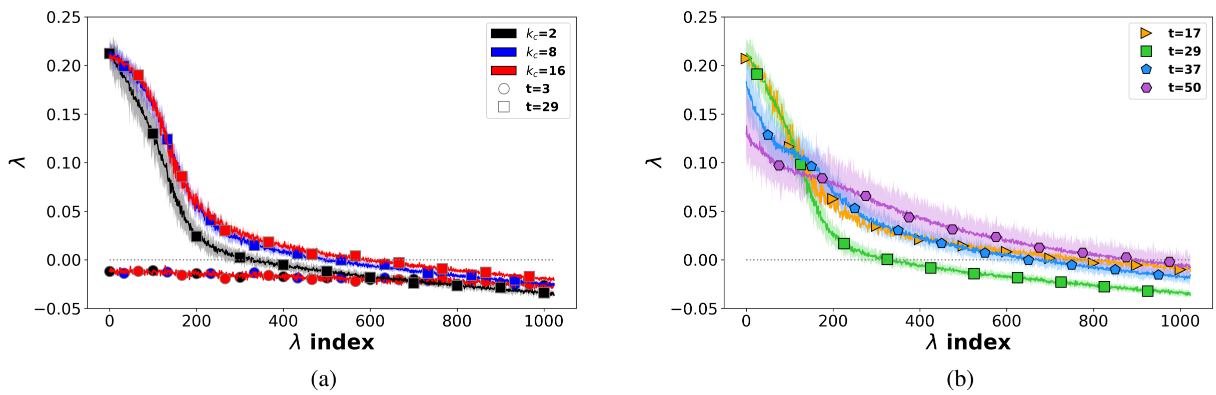

Figure 3: The instantaneous LE spectra are shown in both (a) and (b). The dark lines are the averages of the simulations while the lighter shaded regions show the ranges of values calculated. (a) compares the instantaneous LEs for each value of κ_c at $t = 3$ and $t = 29$. At time $t = 3$, the instantaneous LE spectra appears to be equivalent regardless of the value of κ_c or the random seed used. At $t = 29$, differences between the values of κ_c appear because each are at a different stage of the linear or non-linear regimes. (b) compares the instantaneous LE spectra for $\kappa_c = 2$ at $t = 17$, $t = 29$, $t = 37$, and $t = 50$.

values of κ_c at two different non-dimensional times. At time $t = 3$, the instantaneous spectra appear to be the same between all values of κ_c and random seeds, and remain this way until the respective RTI exits the diffusive regime, which coincides with when the growth rate also deviates. This indicates that perturbations, regardless of the initial conditions, are treated the same in the diffusive regime. Perturbations decay at $t = 3$, as shown by the negative instantaneous LEs. This is surprising because even in the diffusive regime, modes are growing, but perhaps the diffusion at this time is strong enough to remove the small perturbations added to the flow. Although not shown here, the LV at this time $t = 3$ are mostly homogeneous and are not clearly aligned in any specific direction. The lack of a specific direction for the most chaotic LV corresponds to having no positive LEs. Although initially all instantaneous LEs are negative, the first positive LE appears while the RTI is still in the diffusive regime around time $t = 3.40$.

At $t = 29$, the $\kappa_c = 2$ spectra differ significantly from the spectra of the other two values of κ_c. This difference is due to the three values of κ_c being in different regimes of their respective evolutions, as shown in Figure 1. The $\kappa_c = 2$ simulations are in the non-linear regime near the peak growth rate, while the $\kappa_c = 8$ simulations are transitioning between the linear and non-linear regimes, and the $\kappa_c = 16$ simulations are in the linear regime. There is also a much wider range of instantaneous LEs for $\kappa_c = 2$ than for the other two values of κ_c. At $t = 29$, $\kappa_c = 2$ and $\kappa_c = 8$ both consistently show a range of instantaneous LE values for the largest LEs, and the range decreases as the LE index also decreases. $\kappa_c = 16$ has a much smaller range of values, which are inconsistent and the magnitude does not decrease with the LE index. The range of instantaneous LEs appear because they are not time-averaged and the RTI is non-ergodic. Starting at different initial conditions that developed slightly different systems as seen by the differing growth rates will create a range of instantaneous LE values. $\kappa_c = 16$ differs from the other two values of κ_c in its behavior because, at this time, it is only in the linear regime and its growth rate plot does not show a significant difference between the random seeds unlike the other two values of κ_c which are both non-linear and have a spread of growth rate values. When $\kappa_c = 8$ and $\kappa_c = 16$ are both at their peak growth rates, their spectra have a similar shape and spread of values as $\kappa_c = 2$.

Comparison Between Regimes

Although there are some differences in the exact values between the instantaneous LE spectra of the different values of κ_c at similar points in their respective evolutions, the general shapes and the number of positive instantaneous LEs are similar. To determine how the instantaneous LE spectra and the most chaotic LV evolve in time between the different regimes, for simplicity, only $\kappa_c = 2$ will be used. Figure 3a shows the instantaneous LE spectra of $\kappa_c = 2$ in the diffusive regime at $t = 3$ and Figure 3b compares the instantaneous LE spectra of $\kappa_c = 2$ in the linear regime ($t = 17$), in the non-linear regime at the peak growth rate ($t = 29$), later in the non-linear regime ($t = 37$), and in the late-time regime ($t = 50$).

In the early diffusive regime, the instantaneous LEs are all negative and have a slight decreasing trend, but for the most part are around a similar value. After $t = 3.40$, the instantaneous LEs start to become positive, but the values are small and have a small decrease in value. The small variation in the LEs indicates that there is no major direction in which perturbations grow. The many small, positive LEs indicate that the perturbations are weakly growing in the fluid layer in a fairly uniform manner, while the instability is slowly developing.

Around $t = 7$, the instability begins to align itself along specific directions as the largest instantaneous LEs grow in magnitude. Even as the largest LEs begin to grow in magnitude, the smaller LEs do not appear to change until approximately $t = 15$ in the linear regime, when they begin to decrease as the larger LEs continue to increase. $t = 15$ is also around the time when the instability starts to become weakly non-linear because the smallest modes are no longer well described by linear theory when the r.m.s. amplitude becomes greater than $0.1\lambda_{min}$ (Zhou *et al.*, 2021) and saturate when their amplitudes are on the order of their wavelengths (Ramaprabhu *et al.*, 2005).

In the linear regime, most of the instantaneous LEs shown are positive, indicating many degrees of freedom that amplify perturbation growth. This amplification occurs because each mode grows independently of the other modes in the linear regime. Most modes, except the smallest modes, are not saturated at this time, so adding energy to them will amplify them. The instantaneous LEs also appear the same between the different random seeds, so perturbations evolve similarly between each random seed. Figure 4 shows the first LV for one of the random seeds at times $t = 17$, 29, and 50. Figure 4a shows that most of the perturbation growth is localized in the W velocity component and the concentration at $t = 17$. In the linear regime, the majority of the motion is vertical, as the spikes and bubbles form, driven by the buoyancy force from the concentration difference, and no Kelvin-Helmholtz roll-up has occurred yet. The concentration and W velocity component LV magnitudes are concentrated in distinct, unconnected regions where Figure 2a shows the spikes and bubbles are forming and some of their surroundings in the vertical directions. These large concentrated areas indicate that regions not touched by the bubbles and spikes are amplifying perturbations while other regions on the fluid interface do not amplify the perturbations in the concentration and vertical velocity. The regions where perturbations are not amplified appear to correlate where the instability is not growing, or where the fluid interface has not moved.

Unlike the concentration and W velocity component, the U and V velocity components do not have large LV magnitudes. At this early time in the linear regime, this is expected as there is little lateral motion. The U and V velocity components of the first LV are also not structured like the concentration and W velocity component. Instead of large concentrated regions centered at the midplane, the LVs of the U and V velocity components are arranged into top and bottom regions that appear to almost mirror each other. These regions appear to be separated by the fluid interface in Figure 2a and these regions extend beyond the fluid interface. These regions also appear near where the LVs of the concentration and W velocity component show no perturbation growth, or the areas surrounding the fluid interface between the bubbles and spikes of the RTI. These areas have a concentration gradient with a lateral component, possibly causing some of the instability in those regions to have a lateral velocity component.

The velocity components of the LV in Figure 4a at $t = 17$ have many light blue patches surrounding and far from the instability and the white and red regions of large perturbation growth. These light blue regions are similar to those in the LV at $t = 3$, where there is no clear perturbation growth and instead appear to be noise. As the linear regime evolves, these light blue patches shrink, which also corresponds to the shrinking number of positive LEs.

At $t = 29$, the $\kappa_c = 2$ simulations are near the growth rate peak. The instantaneous LE spectra have fewer positive LEs than at $t = 17$. The decrease in the number of positive LEs indicates that the total number of degrees of freedom in which perturbations are growing has also decreased. In Figure 4b at $t = 29$, the light blue region far from the fluid interface has shrunk and instead looks like an artifact of the low resolution. After $t = 29$, the number of positive instantaneous LEs begins to increase again, likely due to the introduction of nonlinearities from secondary instabilities. These secondary instabilities cause the growth rate to decrease and coherent structures to begin to break apart. At $t = 29$, the average instantaneous LEs appear to have the same first 100 values as the spectra at $t = 17$. The similar values between the two times are misleading because at $t = 17$, the instantaneous LEs are increasing in value while at $t = 29$, the exponents are decreasing in value after having reached a maximum near $t = 23$, the time where some larger modes may begin to saturate and the non-linear regime begins. Although the first 100 averaged instantaneous LEs overlap between $t = 17$ and $t = 29$, the instantaneous LEs have a range of values at $t = 29$ that is not seen at $t = 17$.

As the RTI evolves from $t = 29$ to $t = 37$, the instantaneous LE spectra become flatter, with the largest LE values decreasing while the number of positive LEs increases. The largest LE decreases in value, indicating a decrease in the prominence of a specific direction in which perturbations grow the most. At this time, the instability is breaking up as nonlinearities dominant, mixing increases, and the instability becomes more turbulent, introducing broader energy spectra. The increase in mixing increases the sensitivity to perturbations in the U and V velocity components, while the effect of the concentration decreases with the decreasing concentration

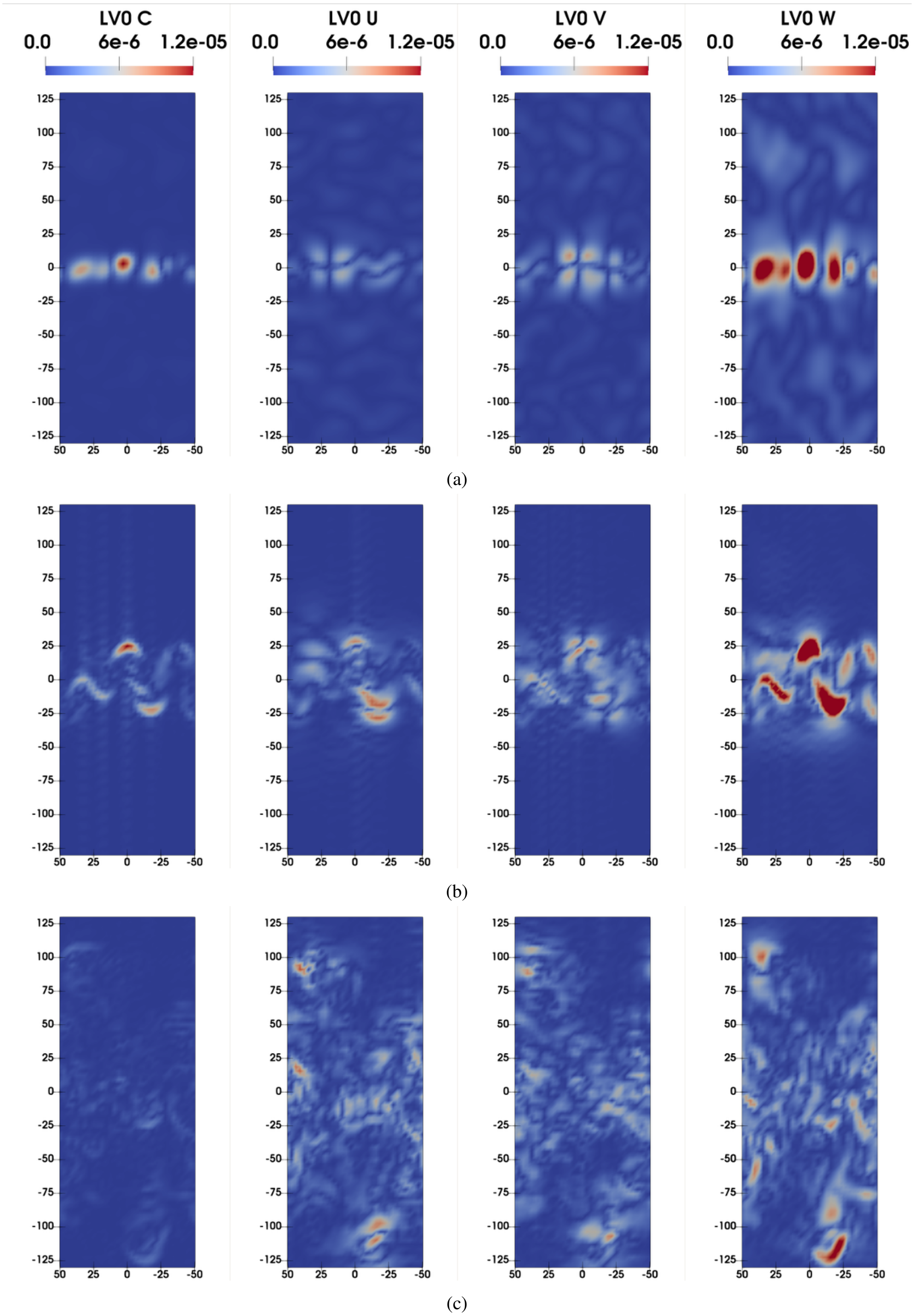

Figure 4: The magnitudes of the first LV at times (a) $t = 17$, (b) $t = 29$, and (c) $t = 50$ for $\kappa_c = 2$ at the mid-plane.

gradient. The range of instantaneous LEs between the different seeds continues to grow.

Lastly, at $t = 50$, the largest LE values continue to decrease in magnitude while the total number of positive LEs increases as the mixing continues to increase and turbulence develops. As the mixing increases, there are more directions that see perturbation growth, but these directions see less pronounced perturbation growth than at earlier times. The change in the perturbation growth can be seen in Figure 4c where there are very few deep red regions of significant perturbation growth, unlike in Figures 4a and 4b. Instead, there is a wide, non-homogeneous region of lower perturbation growth. Most of the perturbation growth is now concentrated in the velocity components, with the concentration seeing barely any perturbation growth. The fluid interface has expanded through diffusion and mixing, and, by this late-time regime, the buoyancy effect due to the concentration gradient has been reduced. Lastly, the range of LE values continues to grow as the instability continues to break apart.

CONCLUSION

This paper investigated the Rayleigh-Taylor instability through a dynamical systems lens using instantaneous LEs and LVs. Although the non-stationary nature of the Rayleigh-Taylor instability limits the use of traditional, time-averaged LEs that are independent of the initial conditions, this work showed that meaningful insight into the RTI can still be gained. The general trends of the LEs were the same regardless of the initial perturbation energy spectrum. Throughout most of the instability, perturbations are amplified, but the strength of the amplification, number of positive LEs, and location of the perturbation growth change throughout the different growth regimes. The diffusive regime saw consistent instantaneous LEs between the different initial conditions and negative values in the beginning.

The continuous presence of positive LEs throughout many of the regimes means that perturbations will grow and affect the flow, possibly removing the effect of the initial conditions. The greatest perturbation growth was seen in the linear and non-linear regimes near the fluid interface. The total number of positive LEs decreases in the non-linear regime until the peak growth rate due to mode saturation and possibly noise reduction, and the total number of positive LEs increases due to the developing secondary instabilities that add additional modes and increase mixing. As the RTI became more turbulent, perturbations grew more uniformly throughout the mixing region. Lastly, as the instability developed, the perturbation growth in the concentration gradually decreased, while the perturbation growth in the U and V velocity components increased.

ACKNOWLEDGMENTS

This research was supported by Los Alamos National Laboratory under the project "Algorithm/Software/Hardware Co-design for High Energy Density applications" at the University of Michigan. This work was also supported by the Center for Prediction, Reasoning, and Intelligence for Multiphysics Exploration (C-PRIME), a PSAAP-IV project funded by the Department of Energy, grant number DE-NA0004264 (program manager: David Etim).

REFERENCES

Benettin, Giancarlo, Galgani, Luigi, Giorgilli, Antonio & Strelcyn, Jean-Marie 1980*a* Lyapunov characteristic exponents for smooth dynamical systems and for hamiltonian systems; a method for computing all of them. part 1: Theory. *Meccanica* **15**, 9–20.

Benettin, Giancarlo, Galgani, Luigi, Giorgilli, Antonio & Strelcyn, Jean-Marie 1980*b* Lyapunov characteristic exponents for smooth dynamical systems and for hamiltonian systems; a method for computing all of them. part 2: Numerical application. *Meccanica* **15**, 21–30.

Cook, Andrew W, Cabot, William & Miller, Paul L 2004 The mixing transition in rayleightaylor instability. *Journal of Fluid Mechanics* **511**, 333–362.

Hassanaly, M. & Raman, V. 2019 Lyapunov spectrum of forced homogeneous isotropic turbulent flows. *Phys. Rev. Fluids* **4**, 114608.

Kalnay, E. 2002 *Atmospheric Modeling, Data Assimilation and Predictability*. Cambridge:Cambridge University Press.

Keefe, L., Moin, P. & Kim, J. 1992 The dimension of attractors underlying periodic turbulent poiseuille flow. *Journal of Fluid Mechanics* **242**, 1–29.

Kord, A. & Capecelatro, J. 2019 Optimal perturbations for controlling the growth of a rayleigh–taylor instability. *Journal of Fluid Mechanics* **876**, 150–185.

Nath, A. V. S., Roy, A., Ravichandran, S. & Govindarajan, R. 2024 Irregular dependence on stokes number, and nonergodic transport, of heavy inertial particles in steady laminar flows. *Phys. Rev. Fluids* **9**, 014302.

Ramaprabhu, P., Dimonte, G. & Andrews, M. J. 2005 A numerical study of the influence of initial perturbations on the turbulent rayleigh–taylor instability. *Journal of Fluid Mechanics* **536**, 285–319.

Ristorcelli, J. R. & Clark, T. T. 2004 Rayleigh–taylor turbulence: self-similar analysis and direct numerical simulations. *Journal of Fluid Mechanics* **507**, 213–253.

Serquina, Ruth, Lai, Ying-Cheng & Chen, Qingfei 2008 Characterization of nonstationary chaotic systems. *Phys. Rev. E* **77**, 026208.

Thévenin, Sébastien & Gréa, Benoît-Joseph 2025 Modeling late-time sensitivity to initial conditions in boussinesq rayleigh–taylor turbulence. *Physica D: Nonlinear Phenomena* **483**, 134947.

Zhou, Ye, Williams, Robin J.R., Ramaprabhu, Praveen, Groom, Michael, Thornber, Ben, Hillier, Andrew, Mostert, Wouter, Rollin, Bertrand, Balachandar, S., Powell, Phillip D., Mahalov, Alex & Attal, N. 2021 Rayleigh–taylor and richtmyer–meshkov instabilities: A journey through scales. *Physica D: Nonlinear Phenomena* **423**, 132838.